

Exploring a New Class of Non-stationary Spatial Gaussian Random Fields with Varying Local Anisotropy

Geir-Arne Fuglstad^{*1}, Finn Lindgren², Daniel Simpson¹, and Håvard Rue¹

¹Department of Mathematical Sciences, NTNU, Norway

²Department of Mathematical Sciences, University of Bath, UK

April 25, 2014

Abstract

Gaussian random fields (GRFs) constitute an important part of spatial modelling, but can be computationally infeasible for general covariance structures. An efficient approach is to specify GRFs via stochastic partial differential equations (SPDEs) and derive Gaussian Markov random field (GMRF) approximations of the solutions. We consider the construction of a class of non-stationary GRFs with varying local anisotropy, where the local anisotropy is introduced by allowing the coefficients in the SPDE to vary with position. This is done by using a form of diffusion equation driven by Gaussian white noise with a spatially varying diffusion matrix. This allows for the introduction of parameters that control the GRF by parametrizing the diffusion matrix. These parameters and the GRF may be considered to be part of a hierarchical model and the parameters estimated in a Bayesian framework. The results show that the use of an SPDE with non-constant coefficients is a promising way of creating non-stationary spatial GMRFs that allow for physical interpretability of the parameters, although there are several remaining challenges that would need to be solved before these models can be put to general practical use.

Keywords: Non-stationary, Spatial, Gaussian random fields, Gaussian Markov random fields, Anisotropy, Bayesian

1 Introduction

Many spatial models for continuously indexed phenomena, such as temperature, precipitation and air pollution, are based on Gaussian random fields (GRFs). This is mainly due to the fact that their theoretical properties are well understood and that their distributions can be fully described by mean and covariance functions. In principle, it is enough to specify the mean at each location and the covariance between any two locations. However, specifying covariance functions is hard and specifying covariance functions that can be controlled by parameters in useful ways is even harder. This is the reason why the covariance function usually is selected from a class of known covariance functions such as the exponential covariance function, the Gaussian covariance function or the Matérn covariance function.

But even when the covariance function is selected from one of these classes, the feasible problem sizes are severely limited by a cubic increase in computation time as a function of the

^{*}Corresponding author, fuglstad@math.ntnu.no

number of observations and a quadratic increase in computation time as a function of the number of prediction locations. This computational challenge is usually tackled either by reducing the dimensionality of the problem (Cressie and Johannesson, 2008; Banerjee et al., 2008), by introducing sparsity in the precision matrix (Rue and Held, 2005) or the covariance matrix (Furrer et al., 2006), or by using an approximate likelihood (Stein et al., 2004; Fuentes, 2007). Sun et al. (2012) offers comparisons of the advantages and challenges associated with the usual approaches to large spatial datasets.

The main goal of this paper is to explore a new class of non-stationary GRFs that provide both an easy way to specify the parameters and allows for fast computations. The main computational tool used is Gaussian Markov random fields (GMRFs) (Rue and Held, 2005) with a spatial Markovian structure where each position is conditionally dependent only on positions close to itself. The strong connection between the Markovian structure and the precision matrix results in sparse precision matrices that can be exploited in computations. The main problem associated with such an approach is that GMRFs must be constructed through conditional distributions, which presents a challenge as it is generally not easy to determine whether a set of conditional distributions gives a valid joint distribution. Additionally, the conditional distributions have to be controlled by useful parameters in such a way that not only the joint distribution is valid, but also such that the effect of the parameters is understood. Lastly, it is desirable that the GMRF is a consistent approximation of a GRF in the sense that when the distances between the positions decrease, the GMRF “approaches” a continuous GRF. These issues are even more challenging for non-stationary GMRFs. It is extremely hard to specify the non-stationarity directly through conditional distributions.

There is no generally accepted way to handle non-stationary GRFs, but many approaches have been suggested. There is a large literature on methods based on the deformation method of Sampson and Guttorp (1992), where a stationary process is made non-stationary by deforming the space on which it is defined. Several Bayesian extensions of the method have been proposed (Damian et al., 2001; 2003; Schmidt and O’Hagan, 2003; Schmidt et al., 2011), but all these methods require replicated realizations which might not be available. There has been some development towards an approach for a single realization, but with a “densely” observed realization (Anderes and Stein, 2008). Other approaches use kernels which are convolved with Gaussian white noise (Higdon, 1998; Paciorek and Schervish, 2006), weighted sums of stationary processes (Fuentes, 2001) and expansions into a basis such as a wavelet basis (Nychka et al., 2002). Conceptually simpler methods have been made with “stationary windows” (Haas, 1990b; 1990a) and with piecewise stationary Gaussian processes (Kim et al., 2005). There has also been some progress with methods based on the spectrum of the processes (Fuentes, 2001; 2002a; 2002b). Recently, a new type of method based on a connection between stochastic partial differential equations (SPDEs) and some classes of GRFs was proposed by Lindgren et al. (2011). They use an SPDE to model the GRF and construct a GMRF approximation to the GRF for computations. An application of a non-stationary model of this type to ozone data can be found in Bolin and Lindgren (2011) and an application to precipitation data can be found in Ingebrigtsen et al. (2013).

This paper extends on the work of Lindgren et al. (2011) and explores the possibility of constructing a non-stationary GRF by varying the local anisotropy. The interest lies both in considering the different types of structures that can be achieved, and how to parametrize the GRF and estimate the parameters in a Bayesian setting. The construction of the GRF is based on an SPDE which describes the GRF as the result of a linear filter applied to Gaussian white noise. Basically, the SPDE expresses how the smoothing of the Gaussian white noise varies at different locations. This construction bears some resemblance to the deformation method of Sampson and Guttorp (1992) in the sense that parts of the spatial variation of the linear filter

can be understood as a local deformation of the space, only with an associated spatially varying variance for the Gaussian white noise. The main idea for computations is that since this filter works locally, it implies a Markovian structure on the GRF. This Markovian structure can be transferred to a GMRF which approximates the GRF, and in turn fast computations can be done with sparse matrices.

This paper presents a first look into a new type of model and the main goal is to explore what can be achieved in terms of models and inference with the model. Section 2 contains the motivation and introduction to the class of non-stationary GRFs that is studied in the other sections. The form of the SPDE that generates the class is given and it is related to more standard constructions of GMRFs. In Section 3 illustrative examples are given on both stationary and non-stationary constructions. This includes some discussion on how to control the non-stationarity of the GRF. Then Section 4 explores parameter estimation for these types of models through different examples with simulated data. The paper ends with discussion of extensions in Section 5 and general discussion and concluding remarks in Section 6.

2 New class of non-stationary GRFs

A GMRF \mathbf{u} is usually parametrized through a mean $\boldsymbol{\mu}$ and a precision matrix \mathbf{Q} such that $\mathbf{u} \sim \mathcal{N}(\boldsymbol{\mu}, \mathbf{Q}^{-1})$. The main advantage of this formulation compared to the usual parametrization of multivariate Gaussian distributions through the covariance matrix is that the Markovian structure is represented in the non-zero structure of the precision matrix \mathbf{Q} (Rue and Held, 2005). Off-diagonal entries are non-zero if and only if the corresponding elements of \mathbf{u} are conditionally independent. This can be seen from the conditional properties of a GMRF,

$$E(u_i | \mathbf{u}_{-i}) = \mu_i - \frac{1}{Q_{i,i}} \sum_{j \neq i} Q_{i,j} (u_j - \mu_j)$$

and

$$\text{Var}(u_i | \mathbf{u}_{-i}) = \frac{1}{Q_{i,i}},$$

where \mathbf{u}_{-i} denotes the vector \mathbf{u} with element i deleted. For a spatial GMRF the non-zeros of \mathbf{Q} can correspond to grid-cells that are close to each other in a grid, neighbouring regions in a Besag model and so on. However, even when this non-zero structure is determined it is not clear what values should be given to the non-zero elements of the precision matrix. This is the framework of the conditionally auto-regressive (CAR) models, whose conception predates the advances in modern computational statistics (Whittle, 1954; Besag, 1974). In the multivariate Gaussian case it is clear that the requirement for a valid joint distribution is that \mathbf{Q} is positive definite, which is not an easy condition to check.

Specification of a GMRF through the conditional properties given above is usually done in a somewhat ad-hoc manner. For regular grids, a process such as random walk can be constructed and the only major issue is to get the conditional variance correct as a function of step-length. For irregular grids the situation is not as clear because each of the conditional means and variances must depend on the varying step-lengths. In Lindgren and Rue (2008) it is demonstrated that some such constructions for second-order random walk can lead to inconsistencies as new grid points are added, and they offer a surprisingly simple construction for second-order random walk based on the SPDE

$$-\frac{\partial^2}{\partial x^2} u(x) = \sigma \mathcal{W}(x),$$

where $\sigma > 0$ and \mathcal{W} is standard Gaussian white noise. If the precision matrix is chosen according to their scheme one does not have to worry about scaling as the grid is refined, as it automatically approaches the continuous second-order random walk. There is an automatic procedure to select the form of the conditional means and variances.

A one-dimensional second-order random walk is a relatively simple example of a process with the same behaviour everywhere. To approximate a two-dimensional, non-stationary GRF, a scheme would require (possibly) different anisotropy and correct conditional variance at each location. To select the precision matrix in this situation poses a large problem and there is abundant use of simple models such as a spatial moving average

$$\mathbb{E}(u_{i,j} | \mathbf{u}_{-\{(i,j)\}}) = \frac{1}{4}(u_{i-1,j} + u_{i+1,j} + u_{i,j-1} + u_{i,j+1})$$

with a constant conditional variance $1/\alpha$. There are ad-hoc ways to extend such a scheme to a situation with varying step-lengths in each direction, but little theory for more irregular choices of locations.

This is why the choice was made to start with the close connection between SPDEs and some classes of GRFs that was presented in Lindgren et al. (2011), which is not plagued by the issues above. From Whittle (1954) it is known that the SPDE

$$(\kappa^2 - \Delta)u(\mathbf{s}) = \mathcal{W}(\mathbf{s}), \quad \mathbf{s} \in \mathbb{R}^2, \quad (1)$$

where $\kappa^2 > 0$ and $\Delta = \frac{\partial^2}{\partial s_1^2} + \frac{\partial^2}{\partial s_2^2}$ is the Laplacian, gives rise to a GRF u with the Matérn covariance function

$$r(\mathbf{s}) = \frac{1}{4\pi\kappa^2}(\kappa\|\mathbf{s}\|)K_1(\kappa\|\mathbf{s}\|),$$

where K_1 is the modified Bessel function of the second kind of order 1. Equation (1) can be extended to fractional operator orders in order to obtain other smoothness parameters in the Matérn covariance function. However, for practical applications, the true smoothness of the field is very hard to estimate from data, in particular when the model is used in combination with an observation noise model. Restricting the development to smoothness 1 in the Matérn family is therefore unlikely to be a major practical serious limitation. However, for practical computations the model will be discretised using methods similar to Lindgren et al. (2011), which does permit other operator orders. Integer orders are easiest, but for stationary models, fractional orders are also achievable (Lindgren et al., 2011, Authors' discussion response). For non-stationary models, techniques similar to Bolin (2013, Section 4.2) would be possible to use. This means that even though we here will restrict the model development to the special case in Equation (1), other smoothnesses, e.g. exponential covariances, will be reachable by combining the different approximation techniques.

The intriguing part, that Lindgren et al. (2011) expanded upon in Equation (1), is that $(\kappa^2 - \Delta)$ can be interpreted as a linear filter acting locally. This means that if the continuously indexed process u were instead represented by a GMRF \mathbf{u} on a grid or a triangulation, with appropriate boundary conditions, one could replace this operator with a matrix, say $\mathbf{B}(\kappa^2)$, only involving neighbours of each location such that Equation (1) becomes approximately

$$\mathbf{B}(\kappa^2)\mathbf{u} \sim \mathcal{N}(0, \mathbf{I}). \quad (2)$$

The matrix $\mathbf{B}(\kappa^2)$ depends on the chosen grid, but after the relationship is derived, the calculation of $\mathbf{B}(\kappa^2)$ is straightforward for any κ^2 . Since $\mathbf{B}(\kappa^2)$ is sparse, the resulting precision matrix $\mathbf{Q}(\kappa^2) = \mathbf{B}(\kappa^2)^T \mathbf{B}(\kappa^2)$ for \mathbf{u} is also sparse. This means that by correctly discretizing the operator (or linear filter), it is possible to devise a GMRF with approximately the same distribution as

the continuously indexed GRF. And because it comes from a continuous equation one does not have to worry about changing behaviour as the grid is refined.

The class of models that are studied in this paper is the one that can be constructed from Equation (1), but with anisotropy added to the Δ operator. A function \mathbf{H} , that gives 2×2 symmetric positive definite matrices at each position, is introduced and the operator is changed to

$$\begin{aligned} \nabla \cdot \mathbf{H}(\mathbf{s})\nabla &= \frac{\partial}{\partial s_1} \left(h_{11}(\mathbf{s}) \frac{\partial}{\partial s_1} \right) + \frac{\partial}{\partial s_1} \left(h_{12}(\mathbf{s}) \frac{\partial}{\partial s_2} \right) \\ &+ \frac{\partial}{\partial s_2} \left(h_{21}(\mathbf{s}) \frac{\partial}{\partial s_1} \right) + \frac{\partial}{\partial s_2} \left(h_{22}(\mathbf{s}) \frac{\partial}{\partial s_2} \right). \end{aligned}$$

This induces different strength of local dependence in different directions, which results in a range that varies with direction at all locations. Further, it is necessary for the discretization procedure to restrict the SPDE to a bounded domain. The chosen SPDE is

$$(\kappa^2 - \nabla \cdot \mathbf{H}(\mathbf{s})\nabla)u(\mathbf{s}) = \mathcal{W}(\mathbf{s}), \quad \mathbf{s} \in \mathcal{D} = [A_1, B_1] \times [A_2, B_2] \subset \mathbb{R}^2, \quad (3)$$

where the rectangular domain makes it possible to use periodic boundary conditions. Neither the rectangular shape of the domain nor the periodic boundary conditions are essential restrictions for the model, but are merely the practical restrictions we choose to work with in this paper, in order to focus on the non-stationarity itself.

When using periodic boundary conditions when approximating the likelihood of a stationary process on an unbounded domain, the parameter estimates will be biased, e.g. when using the Whittle likelihood in the two-dimensional case (Dahlhaus and Künsch, 1987). However, as Lindgren et al. (2011, Appendix A.4) notes for the case with Neumann boundary conditions (i.e. normal derivatives set to zero), the effect of the boundary conditions is limited to a region in the vicinity of the boundary. At a distance greater than twice the correlation range away from the boundary the bounded domain model is nearly indistinguishable from the model on an unbounded domain. Therefore, the bias due to boundary effects can be eliminated by embedding the domain of interest into a larger region, in effect moving the boundary away from where it would influence the likelihood function. For non-stationary models, defining appropriate boundary conditions becomes part of the practical model formulation itself. For simplicity we will therefore ignore this issue here, leaving boundary specification for future development, but provide some additional practical comments in Section 5.

Both for interpretation and for the practical use of Equation (3) it is useful to decompose \mathbf{H} into scalar functions. The anisotropy due to \mathbf{H} is decomposed as

$$\mathbf{H}(\mathbf{s}) = \gamma \mathbf{I}_2 + \mathbf{v}(\mathbf{s})\mathbf{v}(\mathbf{s})^T,$$

where γ specifies the isotropic, baseline effect and the vector field $\mathbf{v}(\mathbf{s}) = [v_x(\mathbf{s}), v_y(\mathbf{s})]^T$ specifies the direction and magnitude of the local, extra anisotropic effect at each location. In this way, one can, loosely speaking, think of different Matérn like fields locally each with its own anisotropy that are combined into a full process. An example of an extreme case of a process with a strong local anisotropic effect is shown in Example 3.2. The example shows that there is a close connection between the vector field and the resulting covariance structure of the GRF.

The main computational challenge is to determine the appropriate discretization of the SPDE in Equation (3), that is how to derive a matrix \mathbf{B} such as in Equation (2). The idea is to look to the field of numerics for discretization methods for differential equations. Then combine these with properties of Gaussian white noise. Namely, that for a Lebesgue measurable subset A of

\mathbb{R}^n , for some $n > 0$,

$$\int_A \mathcal{W}(\mathbf{s}) \, d\mathbf{s} \sim \mathcal{N}(0, |A|),$$

where $|A|$ is the Lebesgue measure of A , and that for two disjoint Lebesgue measurable subsets A and B of \mathbb{R}^n the integral over A and the integral over B are independent (Adler and Taylor, 2007, pp. 24–25). A matrix equation such as Equation (2) was derived for the SPDE in Equation (3) with a finite volume method. The derivations are quite involved and technical and are in Appendix A. However, when the form of the discretized SPDE has been derived as an expression of the coefficients in the SPDE and the grid, the conversion from SPDE to GMRF is automatic for any choice of coefficients and rectangular domain.

3 Examples of models

The simplest case of Equation (3) is with constant coefficients. In this case one has an isotropic model (up to boundary effects) if \mathbf{H} is a constant times the identity matrix or a stationary anisotropic model (up to boundary effects) if this is not the case. In both cases it is possible to calculate an exact expression for the covariance function and the marginal variance for the corresponding SPDE solved over \mathbb{R}^2 .

For this purpose write

$$\mathbf{H} = \begin{bmatrix} H_1 & H_2 \\ H_2 & H_3 \end{bmatrix},$$

where H_1 , H_2 and H_3 are constants. This gives the SPDE

$$\left[\kappa^2 - H_1 \frac{\partial^2}{\partial x^2} - 2H_2 \frac{\partial^2}{\partial x \partial y} - H_3 \frac{\partial^2}{\partial y^2} \right] u(\mathbf{s}) = \mathcal{W}(\mathbf{s}), \quad \mathbf{s} \in \mathbb{R}^2. \quad (4)$$

But if λ_1 and λ_2 are the eigenvalues of \mathbf{H} , then the solution of the SPDE is actually only a rotated version of the solutions of

$$\left[\kappa^2 - \lambda_1 \frac{\partial^2}{\partial \tilde{x}^2} - \lambda_2 \frac{\partial^2}{\partial \tilde{y}^2} \right] u(\mathbf{s}) = \mathcal{W}(\mathbf{s}), \quad \mathbf{s} \in \mathbb{R}^2. \quad (5)$$

Here the new x -axis is parallel to the eigenvector of \mathbf{H} corresponding to λ_1 in the old coordinate system and the new y -axis is parallel to the eigenvector of \mathbf{H} corresponding to λ_2 in the old coordinate system.

From Proposition B.1 one can see that the marginal variance of u is

$$\sigma_m^2 = \frac{1}{4\pi\kappa^2 \sqrt{\det(\mathbf{H})}} = \frac{1}{4\pi\kappa^2 \sqrt{\lambda_1 \lambda_2}}.$$

One can think of the eigenvectors of \mathbf{H} as the two principal directions and λ_1 and λ_2 as a measure of the “strength” of the diffusion in these principal directions. Additionally, if $\lambda_1 = \lambda_2$, which is equivalent to \mathbf{H} being equal to a constant times the identity matrix, the SPDE is rotation and translation invariant and the solution is isotropic. If $\lambda_1 \neq \lambda_2$, the SPDE is still translation invariant, but not rotation invariant, and the solutions are stationary, but not isotropic.

In our case the domain is not \mathbb{R}^2 , but $[0, A] \times [0, B]$ with periodic boundary conditions. This means that a boundary effect is introduced and the above results are only approximately true.

3.1 Stationary models

For a constant \mathbf{H} the SPDE in Equation (3) becomes

$$[\kappa^2 - \nabla \cdot \mathbf{H}\nabla]u(\mathbf{s}) = \mathcal{W}(\mathbf{s}), \quad \mathbf{s} \in [0, A] \times [0, B].$$

This SPDE can be rewritten as

$$[1 - \nabla \cdot \hat{\mathbf{H}}\nabla]u(\mathbf{s}) = \sigma\mathcal{W}(\mathbf{s}), \quad \mathbf{s} \in [0, A] \times [0, B], \quad (6)$$

where $\hat{\mathbf{H}} = \mathbf{H}/\kappa^2$ and $\sigma = 1/\kappa^2$. From this form it is clear that σ is only a scale parameter and that it is enough to solve for $\sigma = 1$ and then multiply the solution with the desired value of σ . Therefore, it is the effect of $\hat{\mathbf{H}}$ that is most interesting to study.

It is useful to parametrize $\hat{\mathbf{H}}$ as

$$\hat{\mathbf{H}} = \gamma\mathbf{I}_2 + \beta\mathbf{v}(\theta)\mathbf{v}(\theta)^T,$$

where $\mathbf{v}(\theta) = [\cos(\theta), \sin(\theta)]^T$, $\gamma > 0$ and $\beta > 0$. In this parametrization one can think of γ as the coefficient of the second order derivative in the direction orthogonal to $\mathbf{v}(\theta)$ and $\gamma + \beta$ as the coefficient of the second order derivative in the direction $\mathbf{v}(\theta)$. Ignoring boundary effects, γ and $\gamma + \beta$ are the coefficients of the second order derivatives in Equation (5) and θ is how much the coordinate system has been rotated in positive direction.

Example 3.1 (Stationary GMRF). The purpose of this example is to consider the effects of using a constant $\hat{\mathbf{H}}$. Use the SPDE in Equation (6) with domain $[0, 20] \times [0, 20]$ and periodic boundary conditions, and discretize with a regular 200×200 grid. Two different values of $\hat{\mathbf{H}}$ are used, an isotropic case with $\hat{\mathbf{H}} = \mathbf{I}_2$ and an anisotropic case with $\gamma = 1$, $\beta = 8$ and $\theta = \pi/4$. The anisotropic case corresponds to a coefficient 9 in the x -direction and a coefficient 1 in the y -direction, and then a rotation of $\pi/4$ in the positive direction. The isotropic GMRF has marginal variances 0.0802 and the anisotropic GMRF has marginal variances 0.0263. For comparison Proposition B.1 gives 0.0796 and 0.0263.

Figure 1 shows one realization for each of the cases. Comparing Figure 1(a) and Figure 1(b) it seems that the direction with the higher coefficient for the second-order derivative has longer range and more regular behaviour. Compared to the corresponding partial differential equation (PDE) without the white noise, this is what one would expect since large values of the coefficient penalize large values of the second order derivatives. One should expect that the correlation range increases when the coefficient is increased.

This is in fact what happens. Figure 2 shows the correlation of the variable at (9.95, 9.95) with every other point in the grid for the isotropic and the anisotropic case. This is sufficient to describe all the correlations since the solutions are stationary. One can immediately note that the iso-correlation curves are close to ellipses with semi-axes along $\mathbf{v}(\theta)$ and the direction orthogonal to $\mathbf{v}(\theta)$. One can see that the correlation decreases most slowly and most quickly in the directions used to specify $\hat{\mathbf{H}}$, with slowest decrease along $\mathbf{v}(\theta)$. It is interesting to see that both the isotropic case and the non-isotropic case has approximately the same length for the minor semi-axis of the iso-correlation curves, and that the major semi-axis is longer for the anisotropic case. This is due to the fact that the lengths of the semi-axes are connected with $\sqrt{\gamma}$ and $\sqrt{\gamma + \beta}$.

From the example above one can see that the use of 3 parameters allow for the creation of GMRFs which are more regular in one direction than the other. One can use the parameters γ , β and θ to control the form of the correlation function and σ to get the desired marginal variance.

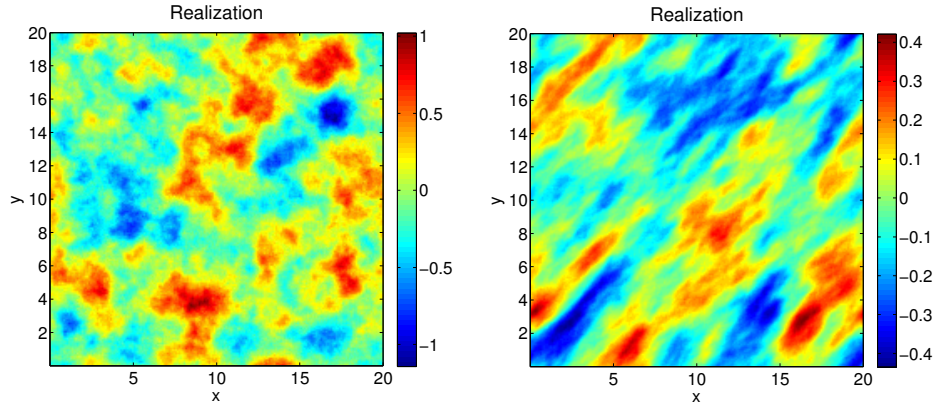


Figure 1: (a) Realization from the SPDE in Example 3.1 on $[0, 20]^2$ with a 200×200 grid and periodic boundary conditions with $\gamma = 1$, $\beta = 0$ and $\theta = 0$. (b) Realization from the SPDE in Example 3.1 on $[0, 20]^2$ with a 200×200 grid and periodic boundary conditions with $\gamma = 1$, $\beta = 8$ and $\theta = \pi/4$.

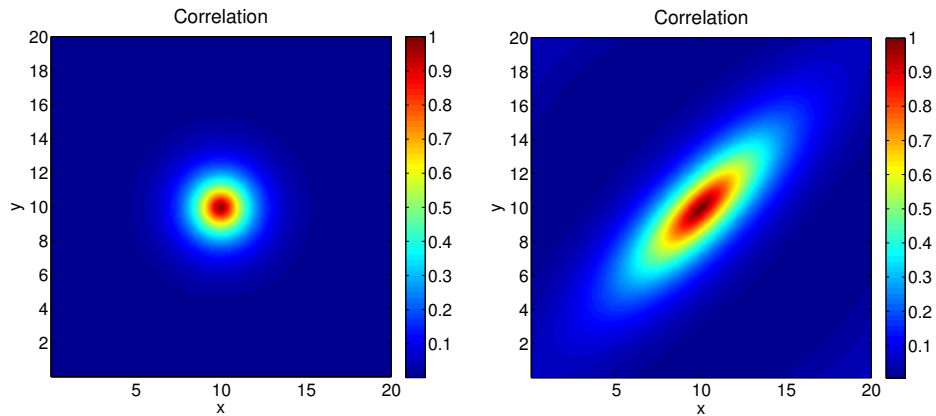


Figure 2: (a) Correlation of the centre with all other points for the solution of the SPDE in Example 3.1 on $[0, 20]^2$ with a 200×200 grid and periodic boundary conditions with $\gamma = 1$, $\beta = 0$ and $\theta = 0$. (b) Correlation of the centre with all other points for the SPDE in Example 3.1 on $[0, 20]^2$ with a 200×200 grid and periodic boundary conditions with $\gamma = 1$, $\beta = 8$, $\theta = \pi/4$.

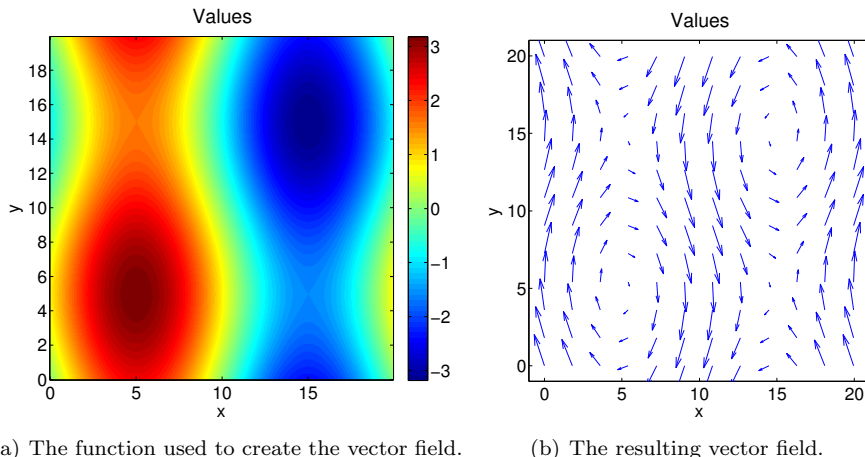


Figure 3: The gradient of the function illustrated in (a) is calculated and rotated 90° counter-clockwise at each point to give the vector field illustrated in (b).

3.2 Non-stationary models

To make the solution of the SPDE in Equation (3) non-stationary, either κ^2 or \mathbf{H} has to be a non-constant function. One way to achieve non-stationarity is by choosing

$$\mathbf{H}(\mathbf{s}) = \gamma \mathbf{I}_2 + \beta \mathbf{v}(\mathbf{s})\mathbf{v}(\mathbf{s})^\top,$$

where \mathbf{v} is a non-constant vector field on $[0, A] \times [0, B]$ which satisfy the periodic boundary conditions and $\gamma > 0$ and $\beta > 0$ are constants.

Example 3.2 (Non-stationary GMRF). Use the domain $[0, 20]^2$ with a 200×200 grid and periodic boundary conditions for the SPDE in Equation (3). Let κ^2 be equal to 1 and let \mathbf{H} be given as

$$\mathbf{H}(\mathbf{s}) = \gamma \mathbf{I}_2 + \beta \mathbf{v}(\mathbf{s})\mathbf{v}(\mathbf{s})^\top,$$

where \mathbf{v} is a 2-dimensional vector field on $[0, 20]^2$ which satisfies the periodic boundary conditions and $\gamma > 0$ and $\beta > 0$ are constants.

To create an interesting vector field, start with the function $f : [0, 20]^2 \rightarrow \mathbb{R}$ defined by

$$f(x, y) = \left(\frac{10}{\pi}\right) \left(\frac{3}{4} \sin(2\pi x/20) + \frac{1}{4} \sin(2\pi y/20)\right).$$

Then calculate the gradient ∇f and let $\mathbf{v} : [0, 20]^2 \rightarrow \mathbb{R}^2$ be the gradient rotated 90° counter-clockwise at each point. Figure 3(a) shows the values of the function f and Figure 3(b) shows the resulting vector field \mathbf{v} . The vector field is calculated on a 400×400 regular grid, because the values between neighbouring cells in the discretization are needed.

Figure 4(a) shows one realization from the resulting GMRF with $\gamma = 0.1$ and $\beta = 25$. A much higher value for β than γ is chosen to illustrate the connection between the vector field and the resulting covariance structure. From the realization it is clear that there is stronger dependence along the directions of the vector field shown in Figure 3(b) at each point than in the other directions. In addition, from Figure 4(b) it seems that positions with large values for the norm of the vector field has smaller marginal variance than positions with small values and

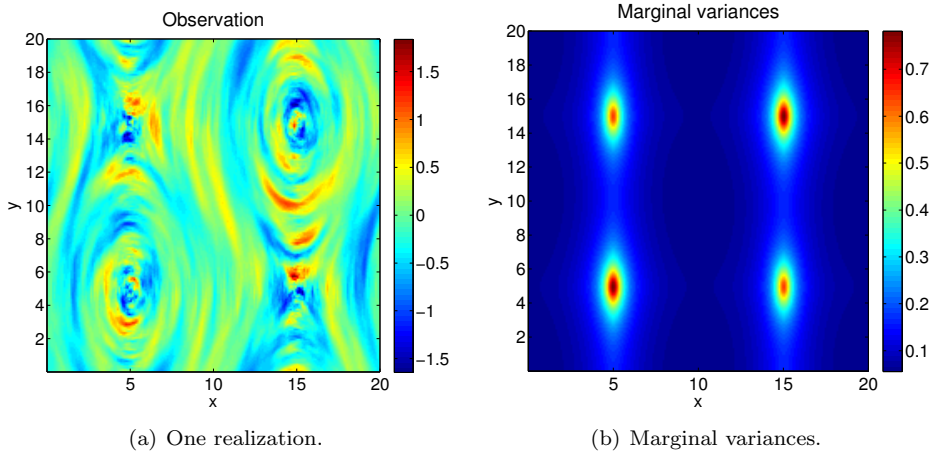


Figure 4: One observation and the marginal variances of the solution of the SPDE in Equation (3) on a 200×200 regular grid of $[0, 20]^2$ with periodic boundary conditions, $\kappa^2 \equiv 1$ and $\mathbf{H} = 0.1\mathbf{I}_2 + 25\mathbf{v}\mathbf{v}^T$, where \mathbf{v} is the vector field described in Example 3.2.

vice versa. This feature introduces an undesired connection between anisotropy and marginal variances. It is possible to reduce this interaction between the vector field and the marginal variances by reformulating the controlling SPDE as discussed briefly in Section 5.

From Figure 5 and Figure 6 one can see that the correlations depend on the direction and norm of the vector field, and that there is clearly non-stationarity. Figure 6(a) and Figure 6(c) show that the correlations with the positions $(4.95, 1.95)$ $(4.95, 7.95)$ tend to follow the vector field around the point $(5, 5)$, whereas Figure 6(b) and Figure 6(d) show that the correlations with the positions $(14.95, 1.95)$ and $(14.95, 7.95)$ tend to follow the vector field away from the point $(15, 5)$. Figure 6(e) shows that the correlations with position $(4.95, 4.95)$ and every other point is not isotropic, but concentrated close to the point itself, and Figure 6(f) shows that the correlations with position $(14.95, 4.95)$ have high correlation along four directions which extends out from the point. Figure 5 shows that the correlations with position $(9.95, 9.95)$ “follow” the vector field with high correlations in the vertical direction.

From this example one can see that allowing \mathbf{H} to be non-constant means that one can vary the dependence structure in more interesting ways than the stationary anisotropic fields. Secondly, using a vector field to control how \mathbf{H} varies means that the resulting correlation structure can be partially visualized from the vector field. Thirdly, when $\gamma > 0$ this construction guarantees that \mathbf{H} is everywhere positive definite.

4 Inference

This section begins with a discussion of the parametrization of the model and the derivation of the posterior distribution. Then the properties of the inference scheme are discussed through some examples with simulated data.

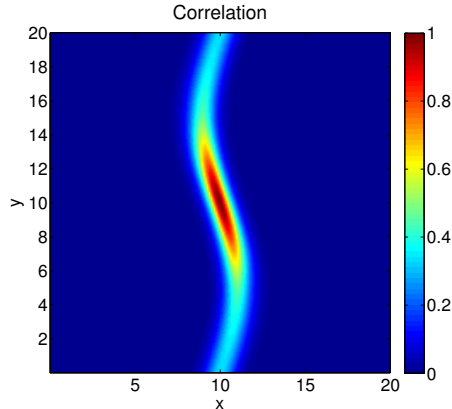


Figure 5: Correlations with position (9.95, 9.95) and all other points for the solution of the SPDE in Example 3.2.

4.1 Posterior distribution and parametrization

The first step for inference is to introduce parameters that control the behaviour of the coefficients in Equation (3) and in turn the behaviour of the GMRF. The way this is done is by expanding each of the functions in a basis and use a linear combination of the basis functions weighted by parameters. For κ^2 only one parameter, say θ_1 , is needed as it is assumed constant, but for the function \mathbf{H} a vector of parameters θ_2 is needed. Set $\theta = (\theta_1, \theta_2^T)$ and give it a prior $\theta \sim \pi(\theta)$. Then for each value of θ , the discretization in Appendix A.3 is used to construct the GMRF $\mathbf{u}|\theta \sim \mathcal{N}(\mathbf{0}, \mathbf{Q}(\theta)^{-1})$. Combine the prior of θ with this conditional distribution to find the joint distribution of the parameters and \mathbf{u} . Together with a model for how an observation \mathbf{y} is made from the underlying GMRF this forms a hierarchical spatial model. The relationship between \mathbf{y} and \mathbf{u} is chosen to be particularly simple, namely that linear combinations of \mathbf{u} are observed with Gaussian noise,

$$\mathbf{y}|\mathbf{u} \sim \mathcal{N}(\mathbf{A}\mathbf{u}, \mathbf{Q}_N^{-1}),$$

where \mathbf{Q}_N is a known precision matrix.

The purpose of the hierarchical model is to do inference on θ based on an observation of \mathbf{y} . With a Gaussian latent model it is possible to integrate out the latent field \mathbf{u} exactly and this leads to the log-posterior

$$\begin{aligned} \log(\pi(\theta|\mathbf{y})) = & \\ & \text{Const} + \log(\pi(\theta)) + \frac{1}{2} \log(|\mathbf{Q}(\theta)|) \\ & - \frac{1}{2} \log(|\mathbf{Q}_C(\theta)|) + \frac{1}{2} \boldsymbol{\mu}_C(\theta)^T \mathbf{Q}_C(\theta) \boldsymbol{\mu}_C(\theta), \end{aligned} \quad (7)$$

where $\mathbf{Q}_C(\theta) = \mathbf{Q}(\theta) + \mathbf{A}^T \mathbf{Q}_N \mathbf{A}$ and $\boldsymbol{\mu}_C(\theta) = \mathbf{Q}_C(\theta)^{-1} \mathbf{A}^T \mathbf{Q}_N \mathbf{y}$. From the above expression one can see that the posterior distribution of θ contains terms which are hard to handle analytically. It is hard to say anything about both the determinants and the quadratic term as functions of θ . Therefore, the inference is done numerically. The model is on a form which could be handled by the INLA methodology (Rue et al., 2009), but at the time of writing the R-INLA software¹

¹www.r-inla.org

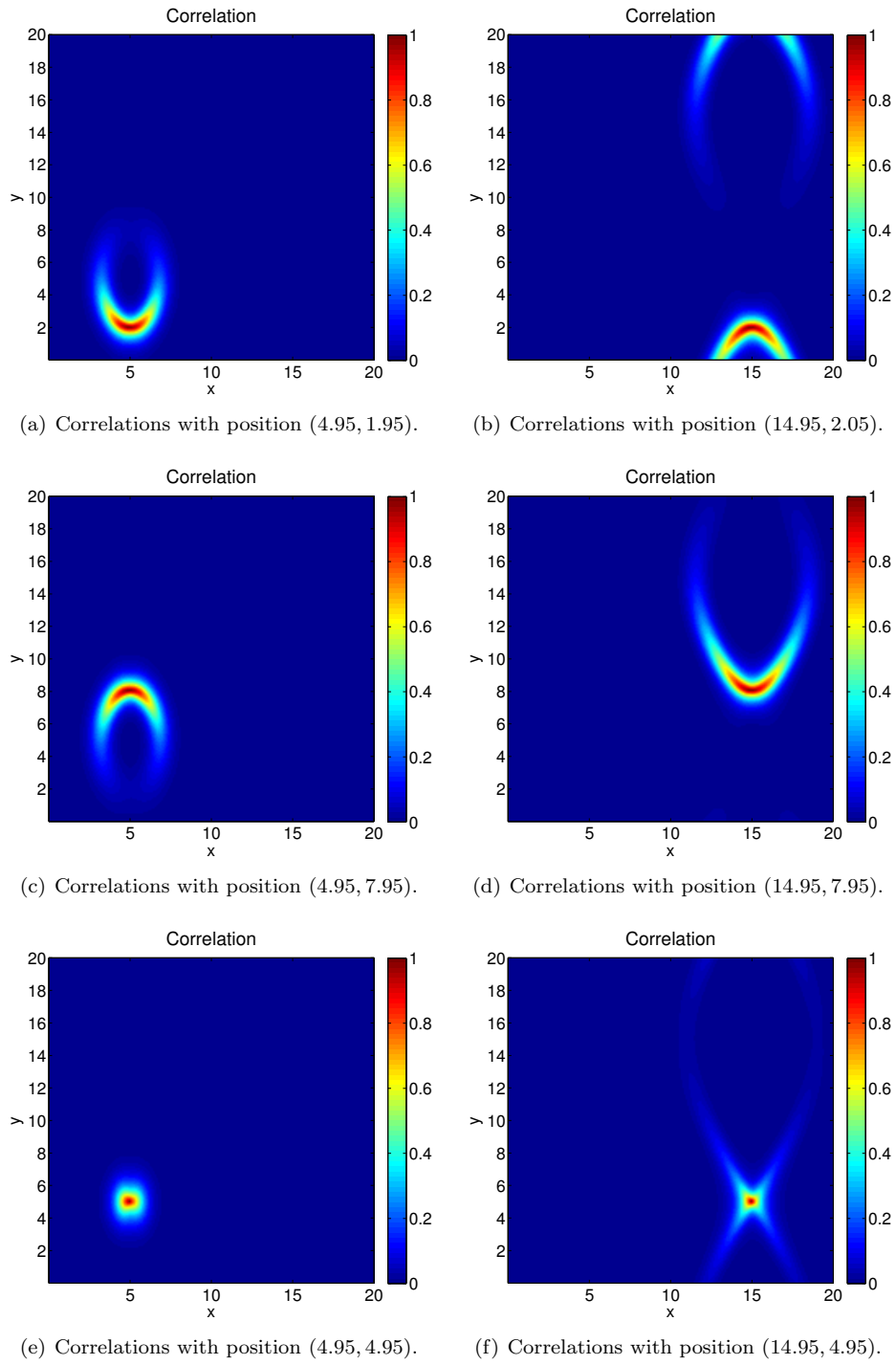


Figure 6: Correlations for different points with all other points for the solution of the SPDE in Example 3.2.

does not have the model implemented. Instead the parameters are estimated with maximum a posteriori estimates based on the posterior density given in Equation (7). In addition, the standard deviations are estimated from the square roots of the diagonal elements of the observed information matrix.

The parametrization of \mathbf{H} introduced in the previous section employs a pre-defined vector field and a parameter β that controls the magnitude of the anisotropy due to this vector field. This is a useful representation for achieving a desired dependence structure, but in an inference setting there may not be any pre-defined vector field to input. Therefore, the vector field itself must be estimated. In this context the decomposition of \mathbf{H} introduced in Section 2,

$$\mathbf{H}(\mathbf{s}) = \gamma \mathbf{I}_2 + \mathbf{v}(\mathbf{s})\mathbf{v}(\mathbf{s})^\top,$$

is more useful. For inference it is necessary to control the vector field by a finite number of parameters. The simple case of a constant matrix requires 3 parameters. Use parameters γ , v_1 and v_2 and write

$$\mathbf{H}(\mathbf{s}) \equiv \gamma \mathbf{I}_2 + \begin{bmatrix} v_1 \\ v_2 \end{bmatrix} \begin{bmatrix} v_1 & v_2 \end{bmatrix}.$$

If \mathbf{H} is not constant, it is necessary to parametrize the vector field \mathbf{v} in some manner. Any vector field is possible for \mathbf{v} , so a basis which can generate any vector field is desirable. The Fourier basis possesses this property, but is only one of many possible choices. Let the domain be $[0, A] \times [0, B]$ and assume that \mathbf{v} is a differentiable, periodic vector field on the domain. Then each component of the vector field can be written as a Fourier series of the form

$$\sum_{(k,l) \in \mathbb{Z}^2} C_{k,l} \exp \left[2\pi i \left(\frac{k}{A}x + \frac{l}{B}y \right) \right],$$

where i is the imaginary unit. But since the components are real-valued, each of them can also be written as a real 2-dimensional Fourier series of the form

$$A_{0,0} + \sum_{(k,l) \in E} \left[A_{k,l} \cos \left[2\pi \left(\frac{k}{A}x + \frac{l}{B}y \right) \right] + B_{k,l} \sin \left[2\pi \left(\frac{k}{A}x + \frac{l}{B}y \right) \right] \right],$$

where the set $E \subset \mathbb{Z}^2$ is given by

$$E = (\mathbb{N} \times \mathbb{Z}) \cup (\{0\} \times \mathbb{N}).$$

Putting these Fourier series together gives

$$\begin{aligned} \mathbf{v}(\mathbf{s}) = & \begin{bmatrix} A_{0,0}^{(1)} \\ A_{0,0}^{(2)} \end{bmatrix} + \sum_{(k,l) \in E} \begin{bmatrix} A_{k,l}^{(1)} \\ A_{k,l}^{(2)} \end{bmatrix} \cos \left[2\pi \left(\frac{k}{A}x + \frac{l}{B}y \right) \right] + \\ & \sum_{(k,l) \in E} \begin{bmatrix} B_{k,l}^{(1)} \\ B_{k,l}^{(2)} \end{bmatrix} \sin \left[2\pi \left(\frac{k}{A}x + \frac{l}{B}y \right) \right], \end{aligned} \quad (8)$$

where $A_{k,l}^{(1)}$ and $B_{k,l}^{(1)}$ are the coefficients for the first component of \mathbf{v} and $A_{k,l}^{(2)}$ and $B_{k,l}^{(2)}$ are the coefficients of the second component. This gives 2 coefficients when only the zero-frequency is included, then 18 parameters when the $(0, 1)$, $(1, -1)$, $(1, 0)$ and $(1, 1)$ frequencies are included. When the number of frequencies used in each direction doubles, the number of required parameters quadruples.

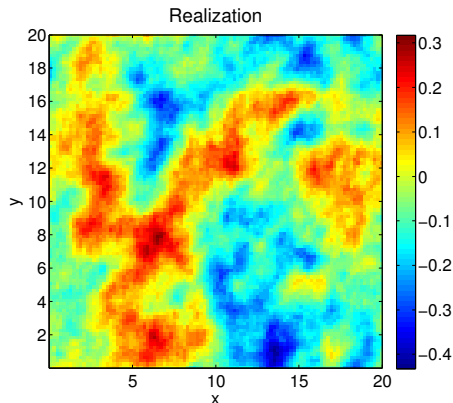


Figure 7: One realization of the solution of the SPDE in Example 4.1.

4.2 Inference on simulated data

In this section we consider data generated from a known set of parameters. The prior used is an improper prior that disallows illegal parameter values. It is uniform on $(0, \infty)$ for γ and uniform on \mathbb{R} for the rest of the parameters in \mathbf{H} . The first issue to investigate is whether it is possible to estimate the stationary model with exactly observed data and whether the approximate estimation scheme performs well.

Example 4.1. Use the SPDE

$$u(\mathbf{s}) - \nabla \cdot \mathbf{H} \nabla u(\mathbf{s}) = \mathcal{W}(\mathbf{s}), \quad \mathbf{s} \in [0, 20] \times [0, 20], \quad (9)$$

where \mathcal{W} is a standard Gaussian white noise process and \mathbf{H} is a 2×2 matrix, with periodic boundary conditions. Let

$$\mathbf{H} = 3\mathbf{I}_2 + 2\mathbf{v}\mathbf{v}^T,$$

with $\mathbf{v} = (1, \sqrt{3})/2$. This means that \mathbf{H} has eigenvector \mathbf{v} with eigenvalue 5 and an eigenvector orthogonal to \mathbf{v} with eigenvalue 3. Construct the GMRF on a 100×100 grid.

One observation of the solution is shown in Figure 7. Assume that the fact that \mathbf{H} is constant is known, but that its value is not. Then using the decomposition from the previous sections one can write

$$\mathbf{H} = \gamma \mathbf{I}_2 + \begin{bmatrix} v_1 \\ v_2 \end{bmatrix} \begin{bmatrix} v_1 & v_2 \end{bmatrix},$$

where γ , v_1 and v_2 are the parameters. Since the process is assumed to be exactly observed, we can use the distribution of $\boldsymbol{\theta} | \mathbf{u}$. This gives the posterior estimates shown in Table 1. From the table one can see that all the estimates are accurate to one digit, and within one standard deviation of the true value. Actually, this decomposition of \mathbf{H} is invariant to changing \mathbf{v} with $-\mathbf{v}$, so there are two choices of parameters that means the same.

The biases in the estimates were evaluated by generating 10000 datasets from the true model and estimating the parameters for each dataset. The estimated bias was less than or equal to 0.1% of the true value for each parameter. Additionally, the sample standard deviations based on the estimation of the parameters for each of the 10000 datasets were 0.070, 0.050 and 0.039 for γ , v_1 and v_2 , respectively. Each one corresponds well to the corresponding approximate standard deviation, computed via the observed information matrix as described in the previous section, that is shown in Table 1.

Table 1: Parameter estimates for Example 4.1.

Parameter	True value	Estimate	Std.dev.
γ	3	2.965	0.070
v_1	0.707	0.726	0.049
v_2	1.225	1.231	0.039

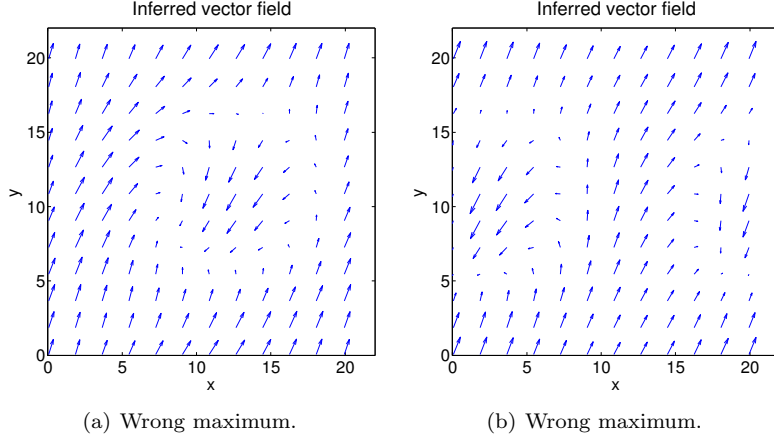


Figure 8: Two different local maxima found for the vector field. The vector field in (a) has a lower value for the posterior distribution of the parameters than the vector field in (b) and both has lower value than the actual maximum.

In the above example it is possible to estimate the model, but this is under the assumption that it is known beforehand that the model is stationary. In general, it is not reasonable to be able to know this beforehand. Therefore, the estimation is repeated for the more complex model developed in the previous sections which allows for significant non-stationarity controlled through a vector field. The intention is to evaluate whether the more complex model is able to detect that the true model is a stationary model and if there are identifiability issues.

Example 4.2. Use the same SPDE and observation as in Example 4.1, but assume that it is not known that \mathbf{H} is constant. Add the terms in the Fourier series corresponding to the next frequencies, $(k, l) = (0, 1)$, $(k, l) = (1, -1)$, $(k, l) = (1, 0)$ and $(k, l) = (1, 1)$. The observation is still assumed to be exact, but there are 16 additional parameters, 4 additional parameters for each frequency.

First two arbitrary starting positions are chosen for the optimization. The first is $\gamma = 3.0$ and all other parameters at 0.1. And the second is $\gamma = 3.0$, $A_{0,0}^{(1)} = 0.1$, $A_{0,0}^{(2)} = 0.1$ and all other parameters equal to 0. For both of these starting points the optimization converges to non-global maximums. Parameter estimates and approximate standard deviations are not show, but Figure 8 shows the two different vector fields found.

A third optimization is done with starting values close to the correct parameter values. This gives a vector field close to the actual one, with estimates for γ , $A_{0,0}^{(1)}$ and $A_{0,0}^{(2)}$ that agree with the ones in Example 4.1 to two digits. The other frequencies all had coefficients close to zero, with the largest having an absolute value of 0.058.

The results illustrate a difficulty with estimation caused by the the inherent non-identifiability of the sign of the vector field. The true vector field is constant and in Figure 8 one can see that

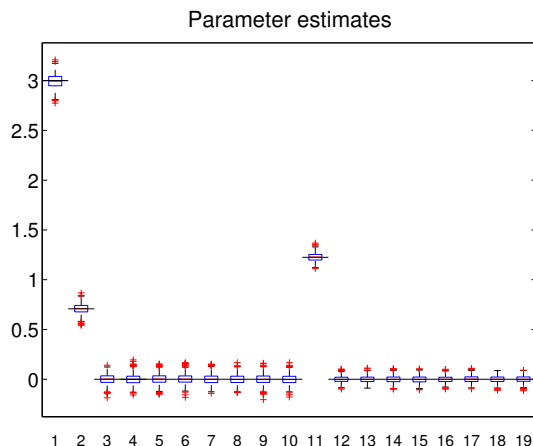


Figure 9: Boxplot of estimated parameters for 1000 simulated datasets in Example 4.2. Parameters 1, 2 and 11 corresponds to γ , v_1 and v_2 , respectively. The red lines inside the boxes specify the medians and the longer black lines through the boxes specify the true parameter values. In most of the boxes the red line is completely covered by the black line.

each vector field has large parts which has the correct appearance if one only considers the lines defined by the arrows and not in which of the two possible directions that the arrow points. The positions where the vector field is wrong are smaller areas where the vector field flips its direction. The problem is that it is difficult to reverse this flipping as it requires moving through states with smaller likelihood. Thus creating undesirable local maximums. One approach to improving the situation would be to force an a priori preference for vector fields without abrupt changes. That is to introduce a prior which forces higher frequencies of the Fourier basis to be less desirable. This is an issue that needs to be addressed for an application and is briefly discussed in Section 5.

By acknowledging the issue and starting close to the true value, one can do repeated simulations of datasets and prediction of parameters to evaluate how well the non-stationary model captures the fact that the true model is stationary and see if there is any consistent bias. 1000 datasets were simulated and the estimation of the parameters was done for each dataset with a starting value close to the true value. This gives the result summarized in the boxplot in Figure 9. There does not appear to be any significant bias and the parameters that give non-stationarity are all close to zero.

The example shows that there are issues in estimating the anisotropy in the non-stationary model due to the non-identifiability of the sign of the vector field, but that if one avoids the local maximums the estimated model is close to the true stationary model in this case. In addition, there is a significant increase in computation time when increasing the parameter space from 3 to 19 parameters. The computation time required is increased by a factor of approximately 10.

A high-dimensional model increases the flexibility, but as seen above also adds additional difficulties. In situations where there is a physical explanation of the additional dependence in one direction, it would be desirable to do a simpler model with one parameter for the baseline isotropic effect and one parameter specifying the degree of anisotropy caused by a pre-defined vector field such as in Example 3.2. This presents a simplification from the previous inference examples because the vector field itself does not need to be estimated.

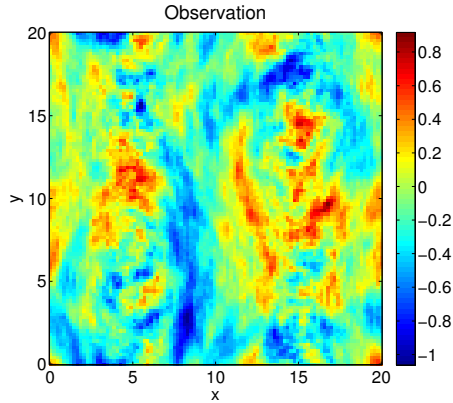


Figure 10: An observation of the SPDE in Equation (3) on a 100×100 regular grid of $[0, 20]^2$ with periodic boundary conditions, $\kappa^2 = 1$ and $\mathbf{H}(\mathbf{s}) = 0.5\mathbf{I}_2 + 5\mathbf{v}(\mathbf{s})\mathbf{v}(\mathbf{s})^\top$, where \mathbf{v} is the vector field in Example 3.2.

Table 2: Posterior inference on parameters in Example 4.3.

Parameter	True value	Estimate	Std.dev.
γ	0.5	0.5012	0.0081
β	5	5.014	0.084

Example 4.3. Use a 100×100 grid of $[0, 20]^2$ and periodic boundary conditions for the SPDE in Equation (3). Let κ^2 be equal to 1 and let \mathbf{H} be parametrized as

$$\mathbf{H}(\mathbf{s}) = \gamma\mathbf{I}_2 + \beta\mathbf{v}(\mathbf{s})\mathbf{v}(\mathbf{s})^\top,$$

where \mathbf{v} is the vector field from Example 3.2.

Figure 10 shows one observation of the solution with $\gamma = 0.5$ and $\beta = 5$. In this case one expects that it is possible to make accurate estimates about γ and β as the situation is simpler than in the previous example.

The estimated parameters are shown in Table 2. From the table one can see that the estimates for both γ and β are quite accurate, which is reflected both in the actual value of the estimates and the approximated standard deviations. The estimates for both γ and β are accurate to 2 digits. In a similar way as in the previous example, the bias is estimated to be less than 0.02% for each parameter, and the sample standard deviation from estimation over many datasets is 0.008 and 0.08 for γ and β respectively.

The above example does not have the same issues as Example 4.2 where the vector field itself must be estimated. The example shows that when using only the $\gamma\mathbf{I}_2$ term and fixed vector field where only the magnitude of the effect is controlled by a parameter β , the estimates of the parameters are quite accurate. The accuracy of the estimates will of course depend on the vector field used.

In a more realistic situation the actual basis needed for the vector field is not known and there is observation noise. In the following example the estimation is compared when all required frequencies are included and when only a subset of the required frequencies of the Fourier basis is included.

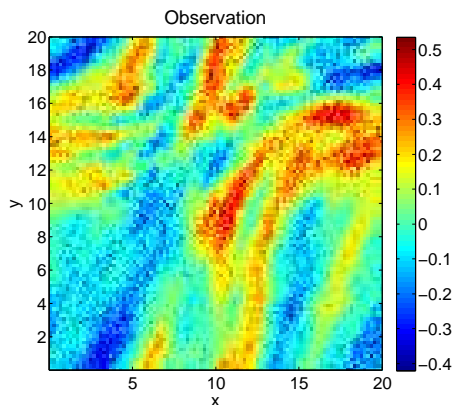


Figure 11: An observation of the SPDE in Example 4.4 with i.i.d. Gaussian white noise with precision 400.

Example 4.4. Use a 100×100 grid of $[0, 20]^2$ and periodic boundary conditions for the SPDE in Equation (3). Let κ^2 be equal to 1 and let \mathbf{H} be given as

$$\mathbf{H}(\mathbf{s}) = \mathbf{I}_2 + \mathbf{v}(\mathbf{s})\mathbf{v}(\mathbf{s})^\top,$$

where \mathbf{v} is the vector field

$$\mathbf{v}(x, y) = \begin{bmatrix} 2 + \cos\left(\frac{\pi}{10}x\right) \\ 3 + 2\sin\left(\frac{\pi}{10}y\right) + \sin\left(\frac{\pi}{10}(x+y)\right) \end{bmatrix}.$$

One observation with i.i.d. Gaussian noise with precision 400 is shown in Figure 11. Based on this realization it is desired to estimate the correct value of γ and the correct vector field \mathbf{v} in the parametrization

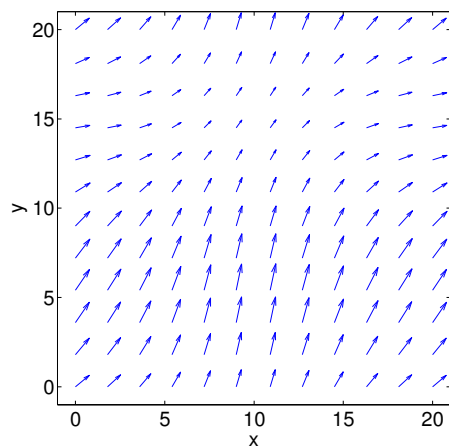
$$\mathbf{H}(\mathbf{s}) = \gamma\mathbf{I}_2 + \mathbf{v}(\mathbf{s})\mathbf{v}(\mathbf{s})^\top.$$

First use only one extra frequency in each direction, that is only the frequencies $(0, 0)$, $(0, 1)$ and $(1, 0)$. This gives the estimated vector field shown in Figure 12(a). Then add the missing frequency and use the frequencies $(0, 0)$, $(0, 1)$, $(1, 0)$ and $(1, 1)$. This gives the estimated vector field shown in Figure 12(b). The true vector field is shown in Figure 12(c).

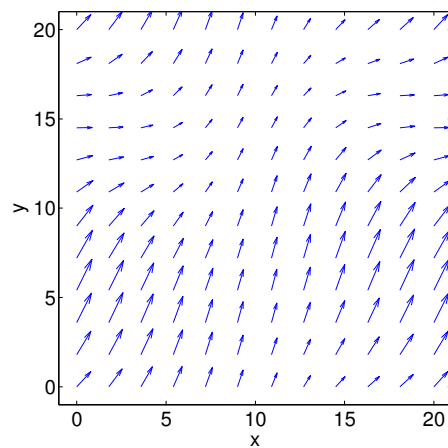
Both estimated vector fields are quite similar to the true vector field, and the γ parameter was estimated to 1.14 in the first case and 1.09 in the latter case. There is a clear bias in the estimate of γ , but this must be expected as there is a need to compensate for the lacking frequencies. All parameter values were estimated, but are not shown. For the first case many parameters is more than two standard deviations from their correct values and in the second case this only happens for one parameter. For each case the difference between the true \mathbf{H} and the estimated $\hat{\mathbf{H}}$ is calculated through

$$\frac{1}{100} \sqrt{\sum_{i=1}^{100} \sum_{j=1}^{100} \left\| \mathbf{H}(\mathbf{s}_{i,j}) - \hat{\mathbf{H}}(\mathbf{s}_{i,j}) \right\|_2^2},$$

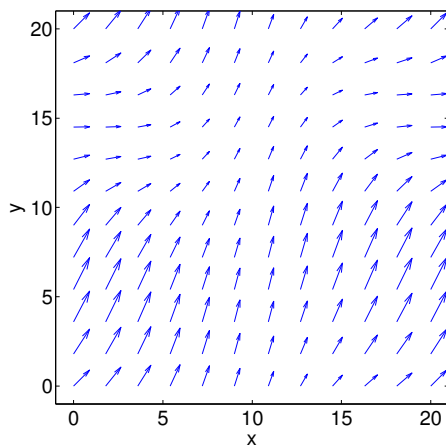
where $\mathbf{s}_{i,j}$ are the centres of the cells in the grid and $\|\cdot\|_2$ denotes the 2-norm. The case with frequencies $(0, 0)$, $(0, 1)$ and $(1, 0)$ gives 7.9 and the case with frequencies $(0, 0)$, $(0, 1)$, $(1, 0)$ and $(1, 1)$ gives 1.5.



(a) $(0,0)$, $(0,1)$ and $(1,0)$ frequencies



(b) $(0,0)$, $(0,1)$, $(1,0)$ and $(1,1)$ frequencies



(c) The true vector field

Figure 12: True vector field and inferred vector fields in Example 4.4. Each of the vector fields is scaled with a factor 0.3.

These examples focus on simple cases where specific issues can be highlighted. The inherent challenges in estimating a spatially varying direction and strength are equally important in the more general setting where also κ and the baseline effect γ is allowed to vary. The estimation of the vector field presents an important component that must be dealt with in any inference strategy for the more general case.

5 Extensions

The class of models discussed in the previous sections offers a flexible way to introduce and control directional dependence at each location using a vector field. This is an important step towards a full flexible non-stationary model for practical applications, but still leaves something to be desired. To make the model applicable to real-world datasets it is necessary to also make the parameters κ and γ spatially varying functions. This results in some control also over the marginal variance and the strength of the local baseline component of the anisotropy at each location. A varying κ is discussed briefly in Section 3.2 in Lindgren et al. (2011).

However, this comes at the cost of two more functions that must be inferred together with the vector field \mathbf{v} . Which in turn means two more functions that need to be expanded into bases. This could be done in a similar way as for the vector field with a Fourier basis, but the Fourier basis does not constitute the only possible choice, and any basis which respects the boundary condition could in principle be used. But the amount of freedom available by having four spatially varying functions comes at a price, and it would be necessary to introduce some apriori restrictions on the behaviour of the functions.

In Example 4.2 the challenge with the non-identifiability of the sign of the vector field is demonstrated. It would be possible to make the situation less problematic by enforcing more structure in the estimated vector field. For example, through spline penalties which adds a preference for components without abrupt changes. Such apriori restrictions make sense both from a modelling perspective, in the sense that the properties should not change too quickly, and from a computational perspective, in the sense that it is desirable to avoid situations as the one encountered in the previous section where the direction of the vector field flips.

The full model could be used in a real-world application through a three step approach. First, choose an appropriate basis to use for each function and select an appropriate prior. This means deciding how many basis elements one is willing to use, from a computational point of view, and how strong the apriori penalties needs to be. Second, find the maximum a posteriori estimate of the functions κ , γ , v_1 and v_2 . Third, assume the maximum a posteriori estimates are the true functions and calculate the predicted values and prediction variances. The full details of such an approach is beyond the scope of this paper and is being studied in current work on an application to annual rainfall data in the conterminous US (Fuglstad et al., 2013).

Another way forward deals with the interactions of the functions κ , γ , v_1 and v_2 . The functions interact in difficult ways to control marginal variance and to control anisotropy. As seen in Example 3.2 the vector field that controls the anisotropic behaviour is also linked to the marginal variances of the field. It would be desirable to try to separate the functions that are allowed to affect the marginal variances and the functions that are allowed to affect the correlation structure. This may present a useful feature in applications, both for interpretability and for constructing priors.

One promising way to greatly reduce this interaction is to extend on the ideas presented in Section 3.4 in Lindgren et al. (2011). The section links the use of an anisotropic Laplacian to the deformation method of Sampson and Guttorp (1992). The link presented is in itself too restrictive, but the last comments about the connection to metric tensors leads to a useful way

to rewrite the SPDE in Equation (3). This is work in progress and involves interpreting the simple SPDE

$$[1 - \Delta]u = \mathcal{W} \tag{10}$$

as an SPDE on a Riemannian manifold with an inverse metric tensor defined through the strength of dependence in different directions in a similar way as the spatially varying matrix \mathbf{H} . This leads to a slightly different SPDE, where a separate function, which does not affect correlation structure, can be used to control marginal standard deviations. However, the separation is not perfect since the varying metric tensor gives a curved space and thus affects the marginal variances of the solution of the above SPDE. But the effect of the metric tensor on marginal standard deviations appears small, and it appears to be a promising way forward.

Another issue which is not addressed in the previous sections is how to define relevant boundary conditions. For rectangular domains, periodic boundary conditions as used here are simple to implement, but a naive use of such conditions will typically not be inappropriate in practical applications due to the resulting spurious dependence between physically distant locations. This problem can be partly rectified by embedding the region of interest into a larger covering domain, so that the boundary effects are moved away from the region that directly influences the likelihood function. It is also possible to apply Neumann type boundary conditions similar to the ones used by Lindgren et al. (2011). These are easier to adapt to more general domains, but they still require a domain extension in order to remove the influence of the boundary condition on the likelihood. A more theoretically appealing, and computationally potentially less expensive, solution would be to directly define the behaviour of the field along the boundary so that the models would contain stationary fields as a neutral case. Work is underway to design stochastic boundary conditions to accomplish this, and some of the solutions show potential for extension to non-stationary models.

6 Discussion

The paper explores different aspects of a new class of non-stationary GRFs based on local anisotropy. The benefit of the formulation presented is that it allows for flexible models with few requirements on the parameters. Since the GRF is based on an SPDE, there is no need to worry about how to change the discretized model in a consistent manner when the grid is refined. In other words, one does not need to worry about how the precision matrix must be changed to give a similar covariance structure when the number of grid points is increased. This is one of the more attractive features of the SPDE-based modelling.

The focus of the examples has been the matrix \mathbf{H} introduced in the Laplace-operator. The examples show that a variety of different effects can be achieved by using different types of spatially varying matrices. Constant matrices of the form $\gamma\mathbf{I}_2$ give isotropic random fields and constant matrices of other forms give anisotropic, stationary random fields. As shown in Section 3 the anisotropic fields have anisotropic Matérn-like covariance functions, through stretching and rotating the domain, and can be controlled by four parameters. It is possible to control the marginal variances, the principal directions and the range in each of the principal directions. A spatially varying \mathbf{H} gives non-stationary random fields. And by using a vector field to specify the strength and direction of extra spatial dependence in each location, there is a clear connection between the vector field and the resulting covariance structure. The covariance structure can be partially visualized from the vector field.

From the examples in Section 4 one can see that sensible values for the parameters are estimated both with and without noise, except for problems with multimodality in Example 4.2, which uses a more flexible construction for the vector field than the other examples. Additionally,

the examples show no significant biases in the estimate. The last example presents the most challenging case, where the true model cannot be represented by the model estimated, and is perhaps closest to a real scenario. In the example good results are achieved when estimating the vector field with only a subset of the frequencies required to fully describe it.

There are many avenues that are not explored in this paper due to the fact that it is a first look into a new type of model. The chief motivation is to explore the class of models both in the sense of what can be achieved and associated challenges for inference with the model. In this paper it is shown that a vector field constitutes a useful way to control local anisotropy in the SPDE-model of Lindgren et al. (2011). What remains for a fully flexible spatial model is to allow also κ and γ to be spatially varying functions. However, this is a simpler task than the anisotropy component since they do not require vector fields. For this more complex model there will be 4 spatially varying functions to estimate and an expansion of each of these functions into a basis will lead to many parameters. This means it is necessary to explore ways of dealing with high-dimensional estimation problems. Additionally, it remains to investigate appropriate choices of priors for use in applications. This question is connected with the discussion in Section 5 on an alternative construction of the model which separates the functions that are allowed to affect marginal variances and the functions that allowed to affect correlation structure.

Acknowledgements

The authors are grateful to Editors and referees for their helpful comments which improved the manuscript.

A Derivation of precision matrix

A.1 Formal equation

The SPDE is

$$(\kappa^2(\mathbf{s}) - \nabla \cdot \mathbf{H}(\mathbf{s}))\nabla u(\mathbf{s}) = \mathcal{W}(\mathbf{s}), \quad \mathbf{s} \in [0, A] \times [0, B], \quad (\text{A.1})$$

where A and B are strictly positive constants, κ^2 is a scalar function, \mathbf{H} is a 2×2 matrix-valued function, $\nabla = \left(\frac{\partial}{\partial x}, \frac{\partial}{\partial y}\right)$ and \mathcal{W} is a standard Gaussian white noise process. In addition, κ^2 is assumed to be a continuous, strictly positive function and \mathbf{H} is assumed to be a continuously differentiable function which gives a positive definite matrix $\mathbf{H}(\mathbf{s})$ for each $\mathbf{s} \in [0, A] \times [0, B]$.

Further, periodic boundary conditions are used, which means that opposite sides of the rectangle $[0, A] \times [0, B]$ are identified. This gives additional requirements for κ^2 and \mathbf{H} . The values of κ^2 must agree on opposite edges and the values of \mathbf{H} and its first order derivatives must agree on opposite edges. The periodic boundary conditions are not essential to the methodology presented in what follows, but were chosen to avoid the issue of appropriate boundary conditions.

A.2 Finite volume methods

In the discretization of the SPDE in Equation (A.1) a finite volume method is employed. The finite volume methods are useful for creating discretizations of conservation laws of the form

$$\nabla \cdot \mathbf{F}(\mathbf{x}, t) = f(\mathbf{x}, t),$$

where $\nabla \cdot$ is the spatial divergence operator. This equation relates the spatial divergence of the flux \mathbf{F} and the sink-/source-term f . The main tool in these methods is the use of the divergence theorem

$$\int_E \nabla \cdot \mathbf{F} \, dV = \oint_{\partial E} \mathbf{F} \cdot \mathbf{n} \, d\sigma, \quad (\text{A.2})$$

where \mathbf{n} is the outer normal vector of the surface ∂E relative to E .

The main idea is to divide the domain of the SPDE in Equation (A.1) into smaller parts and consider the resulting ‘‘flow’’ between the different parts. A lengthy treatment of finite volume methods is not given, but a comprehensive treatment of the method for deterministic differential equations can be found in Eymard et al. (2000).

A.3 Derivation

To keep the calculations simple the domain is divided into a regular grid of rectangular cells. Use M cells in the x -direction and N cells in the y -direction. Then for each cell the sides parallel to the x -axis have length $h_x = A/M$ and the sides parallel to the y -axis have length $h_y = B/N$. Number the cells by (i, j) , where i is the column of the cell (along the x -axis) and j is the row of the cell (along the y -axis). Call the lowest row 0 and the leftmost column 0, then cell (i, j) is

$$E_{i,j} = [ih_x, (i+1)h_x] \times [jh_y, (j+1)h_y].$$

Using this notation the set of cells, \mathcal{I} , is given by

$$\mathcal{I} = \{E_{i,j} : i = 0, 1, \dots, M-1, j = 0, 1, \dots, N-1\}.$$

Figure A.1 shows an illustration of the discretization of $[0, A] \times [0, B]$ into the cells \mathcal{I} .

Each cell has four faces, two parallel to the x -axis (top and bottom) and two parallel to the y -axis (left and right). Let the right face, top face, left face and bottom face of cell $E_{i,j}$ be

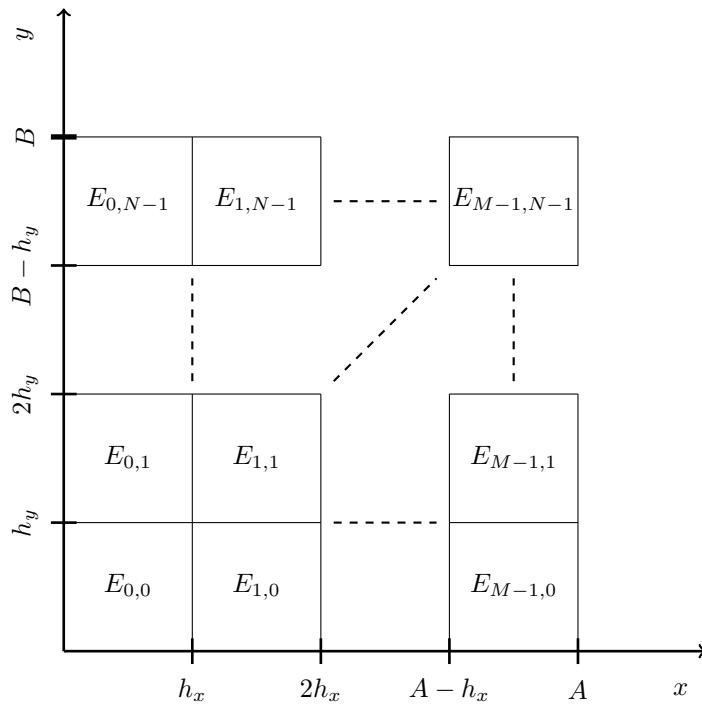


Figure A.1: Illustration of the division of $[0, A] \times [0, B]$ into a regular $M \times N$ grid of rectangular cells.

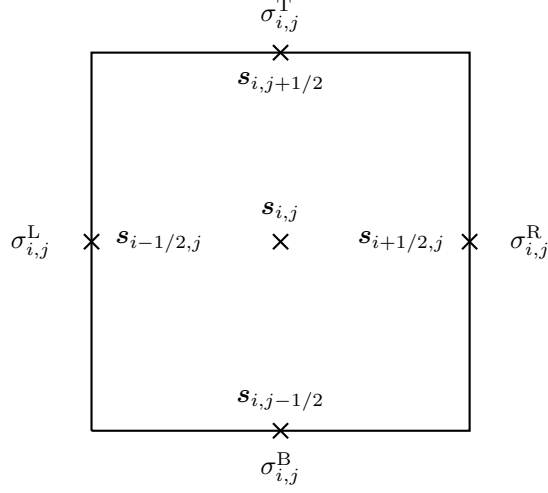


Figure A.2: One cell, $E_{i,j}$, of the discretization with faces $\sigma_{i,j}^R$, $\sigma_{i,j}^T$, $\sigma_{i,j}^L$ and $\sigma_{i,j}^B$, centroid $\mathbf{s}_{i,j}$ and centres of the faces $\mathbf{s}_{i-1/2,j}$, $\mathbf{s}_{i,j-1/2}$, $\mathbf{s}_{i+1/2,j}$ and $\mathbf{s}_{i,j+1/2}$.

denoted $\sigma_{i,j}^R$, $\sigma_{i,j}^T$, $\sigma_{i,j}^L$ and $\sigma_{i,j}^B$, respectively. Additionally, denote by $\sigma(E_{i,j})$ the set of faces of cell $E_{i,j}$.

For each cell $E_{i,j}$, $\mathbf{s}_{i,j}$ gives the centroid of the cell, and $\mathbf{s}_{i+1/2,j}$, $\mathbf{s}_{i,j+1/2}$, $\mathbf{s}_{i-1/2,j}$ and $\mathbf{s}_{i,j-1/2}$ give the centres of the faces of the cell. Due to the periodic boundary conditions, the i -index and j -index in $\mathbf{s}_{i,j}$ are modulo M and modulo N , respectively. Figure A.2 shows one cell $E_{i,j}$ with the centroid and the faces marked on the figure. Further, let $u_{i,j} = u(\mathbf{s}_{i,j})$ for each cell and denote the area of $E_{i,j}$ by $V_{i,j}$. Since the grid is regular, all $V_{i,j}$ are equal to $V = h_x h_y$.

To derive the finite volume scheme, begin by integrating Equation (A.1) over a cell, $E_{i,j}$. This gives

$$\int_{E_{i,j}} \kappa^2(\mathbf{s})u(\mathbf{s}) \, d\mathbf{s} - \int_{E_{i,j}} \nabla \cdot \mathbf{H}(\mathbf{s})\nabla u(\mathbf{s}) \, d\mathbf{s} = \int_{E_{i,j}} \mathcal{W}(\mathbf{s}) \, d\mathbf{s}, \quad (\text{A.3})$$

where $d\mathbf{s}$ is an area element. The integral on the right hand side is distributed as a Gaussian variable with mean 0 and variance V for each (i,j) (Adler and Taylor, 2007, pp. 24–25). Further, the integral on the right hand side is independent for different cells, because two different cells can at most share a common face. Thus Equation (A.3) can be written as

$$\int_{E_{i,j}} \kappa^2(\mathbf{s})u(\mathbf{s}) \, d\mathbf{s} - \int_{E_{i,j}} \nabla \cdot \mathbf{H}(\mathbf{s})\nabla u(\mathbf{s}) \, d\mathbf{s} = \sqrt{V}z_{i,j},$$

where $z_{i,j}$ is a standard Gaussian variable for each (i,j) and the Gaussian variables are independent.

By the divergence theorem in Equation (A.2), the second integral on the left hand side can be written as an integral over the boundary of the cell. This results in

$$\int_{E_{i,j}} \kappa^2(\mathbf{s})u(\mathbf{s}) \, d\mathbf{s} - \oint_{\partial E_{i,j}} (\mathbf{H}(\mathbf{s})\nabla u(\mathbf{s}))^T \mathbf{n}(\mathbf{s}) \, d\sigma = \sqrt{V}z_{i,j}, \quad (\text{A.4})$$

where \mathbf{n} is the exterior normal vector of $\partial E_{i,j}$ with respect to $E_{i,j}$ and $d\sigma$ is a line element. It is

useful to divide the integral over the boundary in Equation (A.4) into integrals over each face,

$$\int_{E_{i,j}} \kappa^2(\mathbf{s})u(\mathbf{s}) \, d\mathbf{s} - (W_{i,j}^R + W_{i,j}^T + W_{i,j}^L + W_{i,j}^B) = \sqrt{V}z_{i,j}, \quad (\text{A.5})$$

where $W_{i,j}^{\text{dir}} = \int_{\sigma_{i,j}^{\text{dir}}} (\mathbf{H}(\mathbf{s})\nabla u(\mathbf{s}))^T \mathbf{n}(\mathbf{s}) \, d\sigma$.

The first integral on the left hand side of Equation (A.5) is approximated by

$$\int_{E_{i,j}} \kappa^2(\mathbf{s})u(\mathbf{s}) \, d\mathbf{s} = V\kappa_{i,j}^2 u(\mathbf{s}_{i,j}) = V\kappa_{i,j}^2 u_{i,j}, \quad (\text{A.6})$$

where $\kappa_{i,j}^2 = \frac{1}{V} \int_{E_{i,j}} \kappa^2(\mathbf{s}) \, d\mathbf{s}$. The function κ^2 is assumed to be continuous and $\kappa_{i,j}^2$ is approximated by $\kappa^2(\mathbf{s}_{i,j})$.

The second part of Equation (A.5) requires the approximation of the surface integral over each face of a given cell. The values of \mathbf{H} are in general not diagonal, so it is necessary to estimate both components of the gradient on each face of the cell. For simplicity, it is assumed that the gradient is constant on each face and that it is identically equal to the value at the centre of the face. On a face parallel to the y -axis the estimate of the partial derivative with respect to x is simple since the centroid of each of the cells which share the face have the same y -coordinate. The problem is the estimate of the partial derivative with respect to y . The reverse is true for the top and bottom face of the cell.

It is important to use a scheme which gives the same estimate of the gradient for a given face no matter which of the two neighbouring cells are chosen. For the right face of $E_{i,j}$, that is $\sigma_{i,j}^R$, the approximation used is

$$\frac{\partial}{\partial y} u(\mathbf{s}_{i+1/2,j}) \approx \frac{1}{h_y} (u(\mathbf{s}_{i+1/2,j+1/2}) - u(\mathbf{s}_{i+1/2,j-1/2})).$$

where the values of u at $\mathbf{s}_{i+1/2,j+1/2}$ and $\mathbf{s}_{i+1/2,j-1/2}$ are linearly interpolated from the values at the four closest cells. More precisely, because of the regularity of the grid the mean of the four closest cells are used. This gives

$$\frac{\partial}{\partial y} u(\mathbf{s}_{i+1/2,j}) \approx \frac{1}{4h_y} (u_{i+1,j+1} + u_{i,j+1} - u_{i,j-1} - u_{i+1,j-1}). \quad (\text{A.7})$$

Note that this formula can be used for the partial derivative with respect to y on any face parallel to the y -axis by suitably changing the i and j indices. The partial derivative with respect to x on a face parallel to the y -axis can be approximated directly by

$$\frac{\partial}{\partial x} u(\mathbf{s}_{i+1/2,j}) \approx \frac{1}{h_x} (u_{i+1,j} - u_{i,j}). \quad (\text{A.8})$$

In more or less exactly the same way the two components of the gradient on the top face of cell $E_{i,j}$ can be approximated by

$$\frac{\partial}{\partial x} u(\mathbf{s}_{i,j+1/2}) \approx \frac{1}{4h_x} (u_{i+1,j+1} + u_{i+1,j} - u_{i-1,j} - u_{i-1,j+1})$$

and

$$\frac{\partial}{\partial y} u(\mathbf{s}_{i,j+1/2}) \approx \frac{1}{h_y} (u_{i,j+1} - u_{i,j}).$$

Table A.1: Finite difference schemes for the partial derivative with respect to x and y at the different faces of cell $E_{i,j}$.

Face	$\frac{\partial}{\partial x}u(s)$	$\frac{\partial}{\partial y}u(s)$
$\sigma_{i,j}^R$	$\frac{u_{i+1,j}-u_{i,j}}{h_x}$	$\frac{u_{i,j+1}+u_{i+1,j+1}-u_{i,j-1}-u_{i+1,j-1}}{4h_y}$
$\sigma_{i,j}^T$	$\frac{u_{i+1,j}+u_{i+1,j+1}-u_{i-1,j}-u_{i-1,j+1}}{4h_x}$	$\frac{u_{i,j+1}-u_{i,j}}{h_y}$
$\sigma_{i,j}^L$	$\frac{u_{i,j}-u_{i-1,j}}{h_x}$	$\frac{u_{i-1,j+1}+u_{i,j+1}-u_{i-1,j-1}-u_{i,j-1}}{4h_y}$
$\sigma_{i,j}^B$	$\frac{u_{i+1,j}+u_{i+1,j-1}-u_{i-1,j-1}-u_{i-1,j}}{4h_x}$	$\frac{u_{i,j}-u_{i,j-1}}{h_y}$

These approximations can be used on any side parallel to the x -axis by changing the indices appropriately.

The approximations for the partial derivatives on each face are collected in Table A.1. Using this table one can find the approximations needed for the second part of Equation (A.5). It is helpful to write

$$W_{i,j}^{\text{dir}} = \int_{\sigma_{i,j}^{\text{dir}}} (\mathbf{H}(\mathbf{s})\nabla u(\mathbf{s}))^T \mathbf{n}(\mathbf{s}) d\sigma = \int_{\sigma_{i,j}^{\text{dir}}} (\nabla u(\mathbf{s}))^T (\mathbf{H}(\mathbf{s})\mathbf{n}(\mathbf{s})) d\sigma,$$

where the symmetry of \mathbf{H} is used to avoid transposing the matrix. Assuming that the gradient is identically equal to the value at the centre of the face, one finds

$$W_{i,j}^{\text{dir}} \approx (\nabla u(\mathbf{c}_{i,j}^{\text{dir}}))^T \int_{\sigma_{i,j}^{\text{dir}}} \mathbf{H}(\mathbf{s})\mathbf{n}(\mathbf{s}) d\sigma,$$

where $\mathbf{c}_{i,j}^{\text{dir}}$ is the centre of face $\sigma_{i,j}^{\text{dir}}$.

Since the cells form a regular grid, \mathbf{n} is constant on each face. Let \mathbf{H} be approximated by its value at the centre of the face, then

$$W_{i,j}^{\text{dir}} \approx m(\sigma_{i,j}^{\text{dir}}) (\nabla u(\mathbf{c}_{i,j}^{\text{dir}}))^T (\mathbf{H}(\mathbf{c}_{i,j}^{\text{dir}})\mathbf{n}(\mathbf{c}_{i,j}^{\text{dir}})), \quad (\text{A.9})$$

where $m(\sigma_{i,j}^{\text{dir}})$ is the length of the face. Note that the length of the face is either h_x or h_y and that the normal vector is parallel to the x -axis or the y -axis.

Let

$$\mathbf{H}(\mathbf{s}) = \begin{bmatrix} H^{11}(\mathbf{s}) & H^{12}(\mathbf{s}) \\ H^{21}(\mathbf{s}) & H^{22}(\mathbf{s}) \end{bmatrix},$$

then using Table A.1 one finds the approximations

$$\begin{aligned} \hat{W}_{i,j}^R &= \\ & h_y \left[H^{11}(\mathbf{s}_{i+1/2,j}) \frac{u_{i+1,j} - u_{i,j}}{h_x} \right] + \\ & h_y \left[H^{21}(\mathbf{s}_{i+1/2,j}) \frac{u_{i,j+1} + u_{i+1,j+1} - u_{i,j-1} - u_{i+1,j-1}}{4h_y} \right], \\ \hat{W}_{i,j}^T &= \\ & h_x \left[H^{12}(\mathbf{s}_{i,j+1/2}) \frac{u_{i+1,j+1} + u_{i+1,j} - u_{i-1,j+1} - u_{i-1,j}}{4h_x} \right] + \\ & h_x \left[H^{22}(\mathbf{s}_{i,j+1/2}) \frac{u_{i,j+1} - u_{i,j}}{h_y} \right], \end{aligned}$$

$$\begin{aligned}\hat{W}_{i,j}^L = & \\ & h_y \left[H^{11}(\mathbf{s}_{i-1/2,j}) \frac{u_{i-1,j} - u_{i,j}}{h_x} \right] + \\ & h_y \left[H^{21}(\mathbf{s}_{i-1/2,j}) \frac{u_{i,j-1} + u_{i-1,j-1} - u_{i-1,j+1} - u_{i,j+1}}{4h_y} \right]\end{aligned}$$

and

$$\begin{aligned}\hat{W}_{i,j}^B = & \\ & h_x \left[H^{12}(\mathbf{s}_{i,j-1/2}) \frac{u_{i-1,j} + u_{i-1,j-1} - u_{i+1,j} - u_{i+1,j-1}}{4h_x} \right] + \\ & h_x \left[H^{22}(\mathbf{s}_{i,j-1/2}) \frac{u_{i,j-1} - u_{i,j}}{h_y} \right].\end{aligned}$$

These approximations can be combined with the approximations in Equation (A.6) and inserted into Equation (A.5) to give

$$V\kappa_{i,j}^2 u_{i,j} - \left(\hat{W}_{i,j}^R + \hat{W}_{i,j}^T + \hat{W}_{i,j}^L + \hat{W}_{i,j}^B \right) = \sqrt{V} z_{i,j}.$$

Stacking the variables $u_{i,j}$ row-wise in a vector \mathbf{u} , that is first row 0, then row 1 and so on, gives the linear system of equations,

$$\mathbf{D}_V \mathbf{D}_{\kappa^2} \mathbf{u} - \mathbf{A}_H \mathbf{u} = \mathbf{D}_V^{1/2} \mathbf{z}, \quad (\text{A.10})$$

where $\mathbf{D}_V = V\mathbf{I}_{MN}$, $\mathbf{D}_{\kappa^2} = \text{diag}(\kappa_{0,0}^2, \dots, \kappa_{M-1,0}^2, \kappa_{0,1}^2, \dots, \kappa_{M-1,N-1}^2)$, $\mathbf{z} \sim \mathcal{N}_{MN}(\mathbf{0}, \mathbf{I}_{MN})$ and \mathbf{A}_H is considered more closely in what follows.

The construction of the matrix \mathbf{A}_H , which depends on the function \mathbf{H} , requires only that one writes out the sum

$$\hat{W}_{i,j}^R + \hat{W}_{i,j}^T + \hat{W}_{i,j}^L + \hat{W}_{i,j}^B$$

and collects the coefficients of the different $u_{a,b}$ terms. This is not difficult, but requires many lines of equations. Therefore, only the resulting coefficients are given. Fix (i,j) and consider the equation for cell $E_{i,j}$. For convenience, let i_p and i_n be the column left and right of the current column respectively and let j_n and j_p be the row above and below the current row respectively. These rows and columns are 0-indexed and due to the periodic boundary conditions one has, for example, that column 0 is to the right of column $M-1$. Further, number the rows and columns of the matrix \mathbf{A}_H from 0 to $MN-1$.

For row $jM+i$ the coefficient of $u_{i,j}$ itself is given by

$$\begin{aligned}(\mathbf{A}_H)_{jM+i,jM+i} = & \\ & - \frac{h_y}{h_x} \left[H^{11}(\mathbf{s}_{i+1/2,j}) + H^{11}(\mathbf{s}_{i-1/2,j}) \right] \\ & - \frac{h_x}{h_y} \left[H^{22}(\mathbf{s}_{i,j+1/2}) + H^{22}(\mathbf{s}_{i,j-1/2}) \right].\end{aligned}$$

The four closest neighbours have coefficients

$$\begin{aligned}
(\mathbf{A}_{\mathbf{H}})_{jM+i, jM+i_p} &= \frac{h_y}{h_x} H^{11}(\mathbf{s}_{i-1/2, j}) - \frac{1}{4} [H^{12}(\mathbf{s}_{i, j+1/2}) - H^{12}(\mathbf{s}_{i, j-1/2})], \\
(\mathbf{A}_{\mathbf{H}})_{jM+i, jM+i_n} &= \frac{h_y}{h_x} H^{11}(\mathbf{s}_{i+1/2, j}) + \frac{1}{4} [H^{12}(\mathbf{s}_{i, j+1/2}) - H^{12}(\mathbf{s}_{i, j-1/2})], \\
(\mathbf{A}_{\mathbf{H}})_{jM+i, j_n M+i} &= \frac{h_x}{h_y} H^{22}(\mathbf{s}_{i, j+1/2}) + \frac{1}{4} [H^{21}(\mathbf{s}_{i+1/2, j}) - H^{21}(\mathbf{s}_{i-1/2, j})], \\
(\mathbf{A}_{\mathbf{H}})_{jM+i, j_p M+i} &= \frac{h_x}{h_y} H^{22}(\mathbf{s}_{i, j-1/2}) - \frac{1}{4} [H^{21}(\mathbf{s}_{i+1/2, j}) - H^{21}(\mathbf{s}_{i-1/2, j})].
\end{aligned}$$

Lastly, the four diagonally closest neighbours have coefficients

$$\begin{aligned}
(\mathbf{A}_{\mathbf{H}})_{jM+i, j_p M+i_p} &= +\frac{1}{4} [H^{12}(\mathbf{s}_{i, j-1/2}) + H^{21}(\mathbf{s}_{i-1/2, j})], \\
(\mathbf{A}_{\mathbf{H}})_{jM+i, j_p M+i_n} &= -\frac{1}{4} [H^{12}(\mathbf{s}_{i, j-1/2}) + H^{21}(\mathbf{s}_{i+1/2, j})], \\
(\mathbf{A}_{\mathbf{H}})_{jM+i, j_n M+i_p} &= -\frac{1}{4} [H^{12}(\mathbf{s}_{i, j+1/2}) + H^{21}(\mathbf{s}_{i-1/2, j})], \\
(\mathbf{A}_{\mathbf{H}})_{jM+i, j_n M+i_n} &= +\frac{1}{4} [H^{12}(\mathbf{s}_{i, j+1/2}) + H^{21}(\mathbf{s}_{i+1/2, j})].
\end{aligned}$$

The rest of the elements of row $jM+i$ are 0.

Based on Equation (A.10) one can write

$$\mathbf{z} = \mathbf{D}_V^{-1/2} \mathbf{A} \mathbf{u},$$

where $\mathbf{A} = \mathbf{D}_V \mathbf{D}_{\kappa^2} - \mathbf{A}_{\mathbf{H}}$. This gives the joint distribution of \mathbf{u} ,

$$\begin{aligned}
\pi(\mathbf{u}) &\propto \pi(\mathbf{z}) \propto \exp\left(-\frac{1}{2} \mathbf{z}^T \mathbf{z}\right) \\
\pi(\mathbf{u}) &\propto \exp\left(-\frac{1}{2} \mathbf{u}^T \mathbf{A}^T \mathbf{D}_V^{-1} \mathbf{A} \mathbf{u}\right) \\
\pi(\mathbf{u}) &\propto \exp\left(-\frac{1}{2} \mathbf{u}^T \mathbf{Q} \mathbf{u}\right),
\end{aligned}$$

where $\mathbf{Q} = \mathbf{A}^T \mathbf{D}_V^{-1} \mathbf{A}$. This is a sparse matrix with a maximum of 25 non-zero elements on each row, corresponding to the point itself, its 8 closest neighbours and the 8 closest neighbours of each of the 8 closest neighbours.

B Marginal variances with constant coefficients

Proposition B.1. *Let u be a stationary solution of the SPDE*

$$\kappa^2 u(x, y) - \nabla \cdot \mathbf{H} \nabla u(x, y) = \mathcal{W}(x, y), \quad (x, y) \in \mathbb{R}^2, \quad (\text{B.1})$$

where \mathcal{W} is a standard Gaussian white noise process, $\kappa^2 > 0$ is a constant, \mathbf{H} is a positive definite 2×2 matrix and $\nabla = \left(\frac{\partial}{\partial x}, \frac{\partial}{\partial y}\right)$.

Then u has marginal variance

$$\sigma_m^2 = \frac{1}{4\pi\kappa^2 \sqrt{\det(\mathbf{H})}}.$$

Proof. Since the solution is stationary, Gaussian white noise is stationary and the SPDE has constant coefficients, the SPDE is acting as a linear filter. Thus one can use spectral theory to find the marginal variance. The transfer function of the SPDE is

$$g(\mathbf{w}) = \frac{1}{\kappa^2 + \mathbf{w}^T \mathbf{H} \mathbf{w}}.$$

Further, the spectral density of a standard Gaussian white noise process on \mathbb{R}^2 is identically equal to $1/(2\pi)^2$. It follows that the spectral density of the solution is

$$f_S(\mathbf{w}) = \left(\frac{1}{2\pi}\right)^2 \frac{1}{(\kappa^2 + \mathbf{w}^T \mathbf{H} \mathbf{w})^2}.$$

From the spectral density it is only a matter of integrating the density over \mathbb{R}^2 ,

$$\sigma_m^2 = \int_{\mathbb{R}^2} f_S(\mathbf{w}) \, d\mathbf{w}.$$

The matrix \mathbf{H} is (symmetric) positive definite and, therefore, has a (symmetric) positive definite square root, say $\mathbf{H}^{1/2}$. Use the change of variables $\mathbf{w} = \kappa \mathbf{H}^{-1/2} \mathbf{z}$ to find

$$\begin{aligned} \sigma_m^2 &= \frac{1}{4\pi^2} \int_{\mathbb{R}^2} \frac{1}{(\kappa^2 + \kappa^2 \mathbf{z}^T \mathbf{z})^2} \det(\kappa \mathbf{H}^{-1/2}) \, d\mathbf{z} \\ &= \frac{1}{4\pi^2 \kappa^2 \sqrt{\det(\mathbf{H})}} \int_{\mathbb{R}^2} \frac{1}{(1 + \mathbf{z}^T \mathbf{z})^2} \, d\mathbf{z} \\ &= \frac{1}{4\pi \kappa^2 \sqrt{\det(\mathbf{H})}}. \end{aligned}$$

□

References

- Adler, R.J. and J.E. Taylor. 2007. *Random Fields and Geometry*, Springer Verlag.
- Anderes, Ethan B and Michael L Stein. 2008. *Estimating deformations of isotropic gaussian random fields on the plane*, The Annals of Statistics, 719–741.
- Banerjee, Sudipto, Alan E. Gelfand, Andrew O. Finley, and Huiyan Sang. 2008. *Gaussian predictive process models for large spatial data sets*, Journal of the Royal Statistical Society: Series B (Statistical Methodology) **70**, no. 4, 825–848.
- Besag, Julian. 1974. *Spatial interaction and the statistical analysis of lattice systems*, Journal of the Royal Statistical Society. Series B (Methodological), 192–236.
- Bolin, D. and F. Lindgren. 2011. *Spatial models generated by nested stochastic partial differential equations, with an application to global ozone mapping*, The Annals of Applied Statistics **5**, no. 1, 523–550.
- Bolin, David. 2013. *Spatial matérn fields driven by non-gaussian noise*, Scandinavian Journal of Statistics. In press.
- Cressie, Noel and Gardar Johannesson. 2008. *Fixed rank kriging for very large spatial data sets*, Journal of the Royal Statistical Society: Series B (Statistical Methodology) **70**, no. 1, 209–226.
- Dahlhaus, R and H Künsch. 1987. *Edge effects and efficient parameter estimation for stationary random fields*, Biometrika **74**, no. 4, 877–882.
- Damian, Doris, Paul D Sampson, and Peter Guttorp. 2001. *Bayesian estimation of semi-parametric non-stationary spatial covariance structures*, Environmetrics **12**, no. 2, 161–178.
- Damian, Doris, Paul D. Sampson, and Peter Guttorp. 2003. *Variance modeling for nonstationary spatial processes with temporal replications*, Journal of Geophysical Research: Atmospheres **108**, no. D24, n/a–n/a.

- Eymard, R., T. Gallouët, and R. Herbin. 2000. *Finite Volume Methods, Solution of Equations in \mathbb{R}^n* (part 3), Techniques of Scientific Computing (Part 3), pp. 713–1018.
- Fuentes, Montserrat. 2001. *A high frequency kriging approach for non-stationary environmental processes*, Environmetrics **12**, no. 5, 469–483.
- . 2002a. *Interpolation of nonstationary air pollution processes: a spatial spectral approach*, Statistical Modelling **2**, no. 4, 281–298, available at <http://smj.sagepub.com/content/2/4/281.full.pdf+html>.
- . 2002b. *Spectral methods for nonstationary spatial processes*, Biometrika **89**, no. 1, 197–210, available at <http://biomet.oxfordjournals.org/content/89/1/197.full.pdf+html>.
- . 2007. *Approximate likelihood for large irregularly spaced spatial data*, Journal of the American Statistical Association **102**, no. 477, pp. 321–331 (English).
- Fuglstad, Geir-Arne, Daniel Simpson, Finn Lindgren, and Håvard Rue. 2013. *Non-stationary Spatial Modelling with Applications to Spatial Prediction of Precipitation*. In preparation.
- Furrer, Reinhard, Marc G Genton, and Douglas Nychka. 2006. *Covariance tapering for interpolation of large spatial datasets*, Journal of Computational and Graphical Statistics **15**, no. 3, 502–523, available at <http://amstat.tandfonline.com/doi/pdf/10.1198/106186006X132178>.
- Haas, Timothy C. 1990a. *Kriging and automated variogram modeling within a moving window*, Atmospheric Environment. Part A. General Topics **24**, no. 7, 1759–1769.
- . 1990b. *Lognormal and moving window methods of estimating acid deposition*, Journal of the American Statistical Association **85**, no. 412, 950–963, available at <http://amstat.tandfonline.com/doi/pdf/10.1080/01621459.1990.10474966>.
- Higdon, David. 1998. *A process-convolution approach to modelling temperatures in the north atlantic ocean*, Environmental and Ecological Statistics **5**, 173–190. 10.1023/A:1009666805688.
- Ingebrigtsen, Rikke, Finn Lindgren, and Ingelin Steinsland. 2013. *Spatial Models with Explanatory Variables in the Dependence Structure of Gaussian Random Fields based on Stochastic Partial Differential Equations*. Submitted.
- Kim, Hyoung-Moon, Bani K Mallick, and C. C Holmes. 2005. *Analyzing nonstationary spatial data using piecewise gaussian processes*, Journal of the American Statistical Association **100**, no. 470, 653–668, available at <http://amstat.tandfonline.com/doi/pdf/10.1198/016214504000002014>.
- Lindgren, Finn and Håvard Rue. 2008. *On the second-order random walk model for irregular locations*, Scandinavian journal of statistics **35**, no. 4, 691–700.
- Lindgren, Finn, Håvard Rue, and Johan Lindström. 2011. *An explicit link between gaussian fields and gaussian markov random fields: the stochastic partial differential equation approach*, Journal of the Royal Statistical Society: Series B (Statistical Methodology) **73**, no. 4, 423–498.
- Nychka, Douglas, Christopher Wikle, and J Andrew Royle. 2002. *Multiresolution models for nonstationary spatial covariance functions*, Statistical Modelling **2**, no. 4, 315–331, available at <http://smj.sagepub.com/content/2/4/315.full.pdf+html>.
- Paciorek, Christopher J. and Mark J. Schervish. 2006. *Spatial modelling using a new class of nonstationary covariance functions*, Environmetrics **17**, no. 5, 483–506.
- Rue, Håvard and Leonard Held. 2005. *Gaussian Markov random fields: Theory and applications*, Monographs on Statistics and Applied Probability, vol. 104, Chapman & Hall, London.
- Rue, Håvard, Sara Martino, and Nicolas Chopin. 2009. *Approximate bayesian inference for latent gaussian models by using integrated nested laplace approximations*, Journal of the Royal Statistical Society: Series B (Statistical Methodology) **71**, no. 2, 319–392.
- Sampson, Paul D. and Peter Guttorp. 1992. *Nonparametric estimation of nonstationary spatial covariance structure*, Journal of the American Statistical Association **87**, no. 417, 108–119, available at <http://www.tandfonline.com/doi/pdf/10.1080/01621459.1992.10475181>.
- Schmidt, Alexandra M., Peter Guttorp, and Anthony O’Hagan. 2011. *Considering covariates in the covariance structure of spatial processes*, Environmetrics **22**, no. 4, 487–500.
- Schmidt, Alexandra M. and Anthony O’Hagan. 2003. *Bayesian inference for non-stationary spatial covariance structure via spatial deformations*, Journal of the Royal Statistical Society: Series B (Statistical Methodology) **65**, no. 3, 743–758.
- Stein, Michael L., Zhiyi Chi, and Leah J. Welty. 2004. *Approximating likelihoods for large spatial data sets*, Journal of the Royal Statistical Society: Series B (Statistical Methodology) **66**, no. 2, 275–296.
- Sun, Ying, Bo Li, and Marc G. Genton. 2012. *Geostatistics for large datasets*, Advances and challenges in space-time modelling of natural events, pp. 55–77. 10.1007/978-3-642-17086-7_3.
- Whittle, P. 1954. *On stationary processes in the plane*, Biometrika **41**, no. 3/4, pp. 434–449 (English).